Pure & Appl. Chem., Vol. 66, No. 6, pp. 1327–1334, 1994.
Printed in Great Britain.
© 1994 IUPAC

Electron cyclotron resonance plasma etching of Si with Cl_2: plasma chemistry and mechanisms

Kouichi Ono, Mutumi Tuda, Hiroki Ootera, and Tatsuo Oomori

Semiconductor Research Laboratory, Mitsubishi Electric Corporation, Tsukaguchi-Honmachi, Amagasaki, Hyogo 661, Japan

Abstract Electron cyclotron resonance (ECR) plasma etching of Si with Cl_2 has been investigated from the viewpoint of plasma chemistry. Experiments were performed over a wide pressure range (0.2–10 mTorr), using a divergent magnetic-field ECR plasma reactor supplied with 2.45-GHz microwave input powers; a floating electrode or substrate holder was located ~30 cm downstream ($B \approx 150$ G) from the 875-G ECR resonance region, and samples of polycrystalline Si were etched with no additional wafer biasing. Several diagnostics were employed to characterize the plasma around the wafer position: two-photon laser-induced fluorescence (LIF), optical emission spectroscopy, microwave interferometry, and electrical measurements with Langmuir probes and a retarding grid analyzer. Moreover, chemical kinetics in Cl_2 plasmas were modeled to gain an insight into the LIF and optical emission measurements, and to know chemical compositions in ECR Cl_2 plasmas. Attention was then focused on neutral Cl atom fluxes and ion energies and fluxes onto the substrate, and on their correlations with the etching characteristics such as etch rates and profiles. The etch rate behavior is interpreted in terms of a modified adsorption-reaction-ion stimulated desorption process, and some lateral etching after an overetch step in terms of the incoming ion trajectories.

1. Introduction

As the integrated circuit device dimensions continue to drop below 0.5 μm and the gate oxide thicknesses drop to 100 Å or less, great demands are still being made on plasma etching technology giving higher directionality, higher selectivity, and less damage. Electron cyclotron resonance (ECR) is one of several plasma-generation techniques that have been developed to meet these demands. Most of such sources are designed to operate at lower gas pressures with magnetic fields, resulting in higher-density, higher-temperature plasmas independent of wafer biasing. To understand and control critical parameters responsible for processing in ECR plasmas, extensive work has focused on the behavior of charged particles such as ions and electrons [1–5]. In contrast, little or no attention has been paid to reactive neutrals, which are generally assumed to play an important role in many etching processes; in effect, it may be difficult to quantitatively measure the concentrations of reactive neutral species under typical ECR processing conditions.

This paper presents plasma chemical aspects of the ECR chlorine plasma etching of Si; in practice, Si etching with Cl_2 is not only a relatively simple process, but also an important one to achieve highly directional, highly selective etching of Si over SiO_2 without surface inhibitors. In our studies, the concentrations of atomic Cl, the principal neutral reactant in Cl_2 plasmas, were measured by two-photon laser-induced fluorescence (LIF) [6]. Modeling calculations of chemical kinetics in ECR Cl_2 plasmas were also made taking account of a number of electron-impact events and ion reactions. The numerical results gave a quantitative understanding of chemical compositions in ECR plasmas, being compared with the measured Cl concentrations. These results, together with electrical measurements of ion and electron energies and densities, yielded neutral Cl fluxes and ion energies and fluxes onto the substrate, which are reduced parameters that primarily govern the etching characteristics. Moreover, a modified adsorption-reaction-ion stimulated desorption process is discussed to interpret the Si etch rate behavior,

and some lateral etching observed after an overetch step is interpreted in terms of the incoming ion trajectories affected by localized charging of pattern features. This is a preliminary effort to qualify the role of reactive neutrals as well as that of ions in low-pressure, high-density plasma processing.

2. Experiment

Figure 1 shows the experimental setup which has been detailed elsewhere [5,6]. Briefly, the ECR plasma reactor consisted of two grounded stainless-steel chambers: a water-cooled plasma chamber 20 cm in diameter and 50 cm long, and a specimen chamber 35 cm in diameter and 45 cm long. Four solenoid coils were set around the former, providing a divergent magnetic field to produce ECR plasmas and transport them to a sample for etching in the specimen chamber. The discharge was established by 2.45-GHz right-hand circularly polarized microwaves of TE_{11} mode, fed to the plasma chamber via a 10-cm-diam quartz window; the 875-G ECR resonance was located at an axial position $z \approx 42$ cm from the microwave entrance, near the end of the plasma chamber. Pure Cl_2 gas was introduced into the reactor, evacuated down to a base pressure $<10^{-6}$ Torr, through a set of small holes around the entrance window. The specimen chamber had an end port for pumping and side ports for diagnostics, containing a 17-cm-diam floating electrode or substrate holder at $z \approx 75$ cm, ~33 cm downstream ($B \approx 150$ G) from the ECR resonance region. Experiments were performed at an incident microwave power of 900 W (0.068 W/cm^3) and a Cl_2 gas flow rate of 10 standard cm^3/min; the reactor gas pressure was varied from P_0=10 to 0.2 mTorr (1.33 to 0.0266 Pa), and the corresponding gas residence time in the specimen chamber was estimated to be of the order of $\tau_r \approx 3.4$–0.068 s.

Several diagnostics were employed to characterize the plasma around the wafer position: two-photon LIF, optical emission spectroscopy, microwave interferometry, and electrical measurements with Langmuir probes and a retarding grid analyzer. The LIF measurements sampled a portion of the discharge on axis ~2.5 cm upstream from the electrode. In our LIF measurements [6], ground-state Cl atoms were excited by two-photon absorption of 233.2-nm laser radiation, and the fluorescence of Cl was observed at 725.6 nm. Absolute calibration was achieved to obtain the Cl concentrations, by generating Cl atoms through UV photolysis of CCl_4 molecules with the same laser radiation. A microwave interferometer operated at 24 GHz was used to monitor the line-averaged plasma electron density, and optical emissions were also monitored routinely in these experiments. Moreover, planar Langmuir probes were employed to measure the ion density, electron temperature, and the plasma and floating potentials. A retarding grid analyzer was set in place of the substrate holder, measuring the flux and energy distribution of positive ions directed toward the substrate on axis [5].

Samples for etching were 6-in.-diam single-crystal Si wafers with a 1000-Å-thick layer of thermally grown SiO_2 and then a 3000-Å-thick layer of heavily P-doped polycrystalline Si, masked with a 1-μm-thick photoresist pattern of lines and spaces. The samples were clamped into place on the electrode whose temperature was controlled by circulating coolant fluid, and backside helium was injected for increased wafer thermal contact. The etched depth was measured by a stylus gauge, and the vertical etch rate was calculated as the ratio of the etched depth to the total etching time. Moreover, the etched profile was examined with a scanning electron microscope (SEM). In these experiments, prior to main etching under floating substrate conditions, an additional rf biasing at 13.56 MHz was used during a brief pre-etch breakthrough step to remove a native oxide layer.

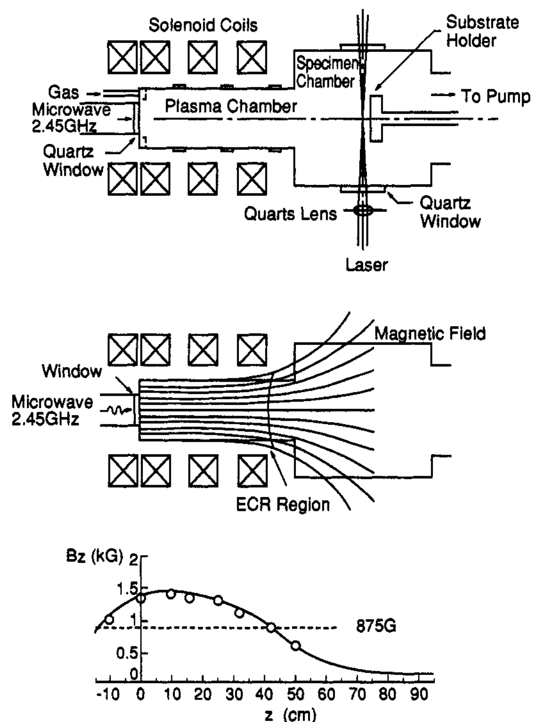

Fig. 1 Experimental setup.

3. Results of Plasma Characterization

Figure 2 shows the electrical measurements of ion and electron energies and densities on axis around the wafer position as a function of Cl_2 pressure P_0: (a) the plasma electron density n_e and temperature T_e; (b) the plasma potential V_p and the difference V_p-V_f between the plasma and floating potentials; and (c) the ion flux Γ_i and the peak ion energy E_i toward the substrate. Here, the ion energies E_i measured by a retarding grid analyzer are in agreement with the potential differences V_p-V_f measured by a Langmuir probe, which correspond to the sheath potentials V_s at the floating substrate. Moreover, the measured ion fluxes Γ_i are consistent with the Γ_i values calculated using the Bohm criterion [7] with the measured n_i ($\approx n_e$) and T_e: $\Gamma_i = 0.6n_i(kT_e/m_i)^{1/2}$, where n_i is the ion density, k is Boltzmann's constant, and m_i is the ion mass (assuming Cl_2^+ ions are predominant). As P_0 is decreased, the plasma density increases form $n_e \approx 10^{10}$ to 10^{11} cm^{-3}, peaks at $P_0 \approx 0.4$ mTorr, and then decreases; the electron temperature increases continuously from $T_e \approx 2.5$ to 9 eV. Correspondingly, the plasma potential V_p and the potential difference V_p-V_f increase significantly with decreasing P_0. The ion energy ranges from $E_i \approx 10$ to 70 eV, and the ion flux toward the substrate ranges from $\Gamma_i \approx 0.16$ to 2.5 mA/cm^2, corresponding to ≈ 0.10 to 1.6×10^{16} ions/cm^{2}s.

The optical emission intensities of several atomic lines and molecular bands of Cl, Cl^+, Cl_2, and Cl_2^+, measured around the wafer position, are also shown in Fig. 2(d). It is noted here that the emission intensity of Cl_2 decreases with decreasing P_0, while that of Cl^+ increases significantly; on the other hand, the Cl and Cl_2^+ intensities exhibit relatively little changes over the P_0 range studied. The decreased Cl_2 intensity at lowered P_0 may be related to a decrease in the feedstock Cl_2 gas density, and the increased Cl^+ intensity to an increase in T_e.

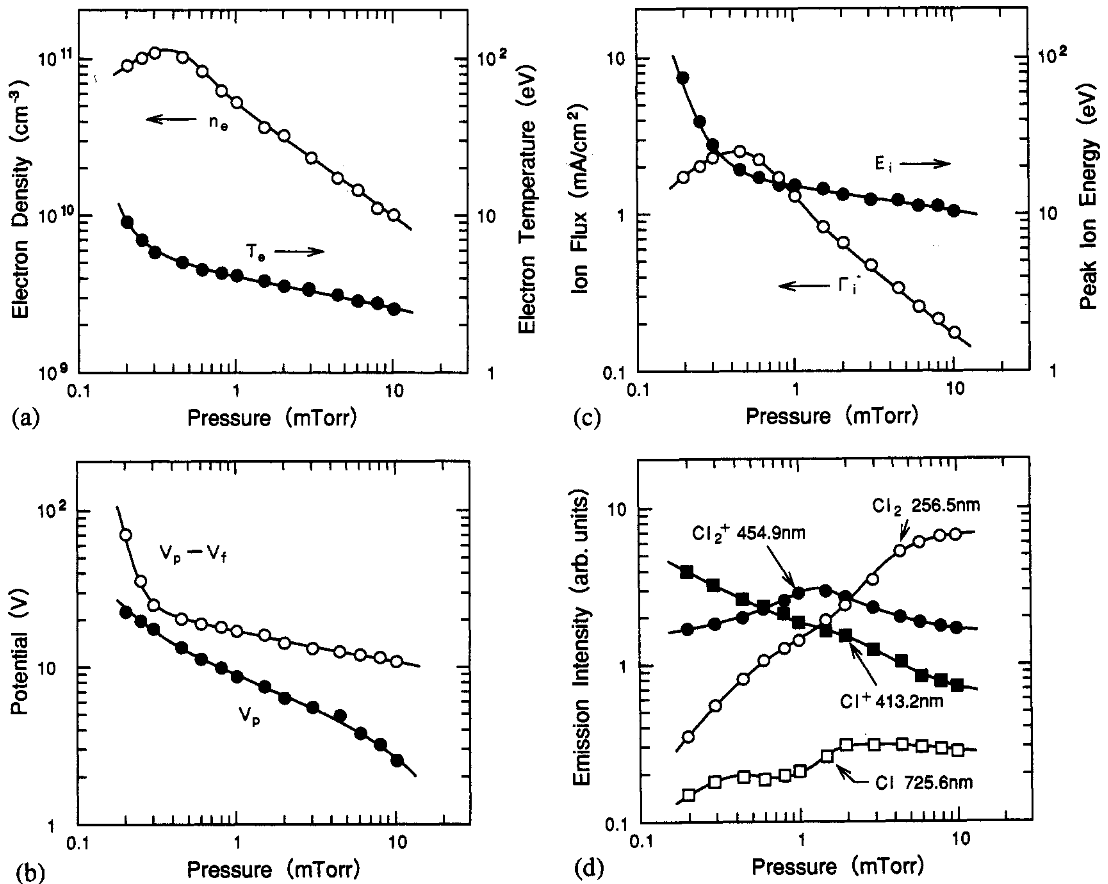

Fig. 2 (a) Plasma electron density n_e and temperature T_e, (b) plasma potential V_p and difference V_p-V_f between the plasma and floating potentials, (c) ion flux Γ_i and peak ion energy E_i toward the substrate, and (d) optical emission intensities of several atomic lines and molecular bands of chlorine, measured around the wafer position as a function of Cl_2 pressure P_0.

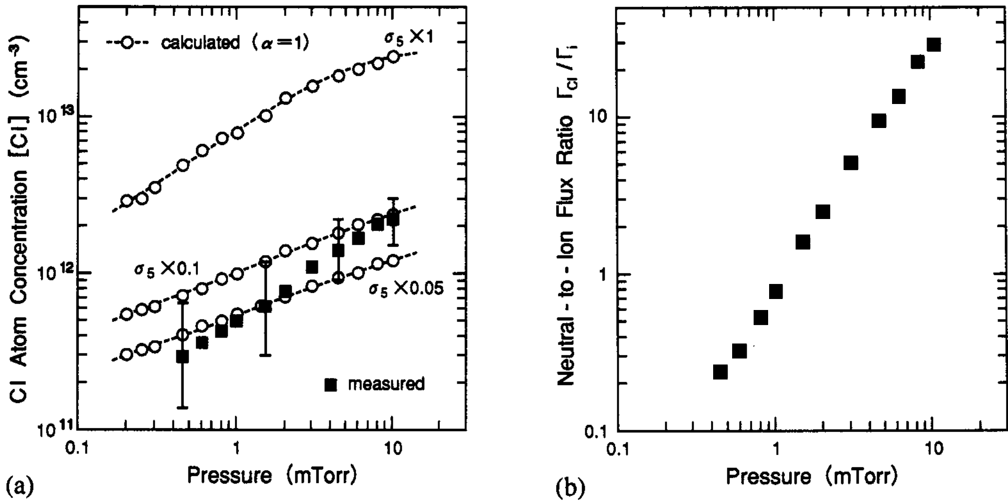

Fig. 3 (a) Cl atom concentration [Cl] and (b) ratio Γ_{Cl}/Γ_i of neutral Cl flux to ion flux toward the substrate as a function of Cl_2 pressure P_0. In (a), the solid squares are the two-photon LIF measured data on axis around the wafer position, while the open circles represent the results of modeling calculations of chlorine chemical kinetics.

Figure 3(a) shows the Cl atom concentration [Cl] as a function of Cl_2 pressure P_0. Here, the solid squares represent the measured data on axis around the wafer position by two-photon LIF; the measurement and absolute calibration techniques have been detailed in [6]. Unfortunately, our LIF measurements could not be made at lower pressures, P_0<0.5 mTorr, owing to deteriorated signal-to-noise problems due to increased fluctuation of increased background plasma emission. The Cl concentration measured ranges from [Cl]$\approx 2\times10^{12}$ to 3×10^{11} cm^{-3}, decreasing with decreasing P_0. The corresponding Cl fractions, [Cl]/[Cl_2], are estimated to be between $\approx$1 and 2 % (assuming the gas temperature T=300 K). From the concentration of Cl atoms and their thermal velocity, the flux Γ_{Cl} of Cl atoms directed to the substrate can be calculated as $\Gamma_{Cl} = (1/4)[Cl](8kT/\pi m)^{1/2}$, assuming [Cl] to be uniform in space. The neutral Cl flux thus calculated ranges from $\Gamma_{Cl} \approx$ 3 to 0.4×10^{16} atoms/cm^{2}s.

The ratio of ion flux to neutral flux striking the substrate, or its inverse, is one of reduced parameters that primarily govern the etch rate and anisotropy. From the above Cl concentration measurements and the electrical measurements of ion and electron energies and densities in Fig. 2, the ratio of neutral Cl flux to ion flux toward the substrate, Γ_{Cl}/Γ_i, can be evaluated as shown in Fig. 3(b). Our measurements demonstrate that the neutral-to-ion flux ratio in ECR decreases almost linearly with decreasing pressure, from $\Gamma_{Cl}/\Gamma_i \approx$ 30 at P_0=10 mTorr to 0.3 at P_0=0.5 mTorr.

4. Chemical Kinetics Model

A preliminary model of chemical kinetics in ECR Cl_2 plasmas was assembled from reactions which have been known in the literature, together with others assumed to occur by comparison with reactions of homologous molecules. The species included in the model are Cl_2, Cl, Cl_2^+, Cl^+, Cl^{++}, and Cl^-, and a summary of their electron-impact events and ion reactions are listed in Table 1, together with the excitation thresholds E_{th}. In ECR plasmas, electron-ion recombination processes, except dissociative one, may be unimportant owing to high electron temperatures T_e; the electron attachment, leading to Cl_2^- negative ions, is also unlikely to occur in binary electron-molecule collisions at low pressures P_0.

Cross sections for the reaction processes concerned here are not well known. As for electron-impact events, only the following shown in Fig. 4 have been directly measured as a function of electron energy E_e: Q_i (=$\sigma_1+\sigma_2+\sigma_3$), the total ionization cross section for Cl_2 [8]; Q_a (=$\sigma_3+\sigma_4$), the total cross section for negative-ion formation from Cl_2 [8]; σ_6, the cross section for ionization of Cl [9]; and σ_7, the cross section for ionization of Cl^+ [10]. The respective cross sections σ_x (x=1–4) for ionization and attachment may be determined as follows, from the Q_i and Q_a on referring to relative photoionization yields of Cl_2^+, Cl^+, and Cl^- from Cl_2 in the vacuum UV [11,12]: $\sigma_1=Q_i-(\sigma_2+\sigma_3)$, $\sigma_2=Q_i(E_e-4.0)/4$, $\sigma_3=Q_a$

TABLE 1. Cl/Cl_2 reaction processes in chlorine plasmas.

Reaction process		E_{th} (eV)	σ (cm^2)	k (cm^3/s)
Molecular ionization	$e+Cl_2 \rightarrow Cl_2^+ + e + e$	11.48	σ_1	k_1
Dissociative ionization	$e+Cl_2 \rightarrow Cl^+ + Cl + e + e$	15.48	σ_2	k_2
Ion-pair formation	$e+Cl_2 \rightarrow Cl^+ + Cl^- + e$	11.87	σ_3	k_3
Dissociative attachment	$e+Cl_2 \rightarrow (Cl_2^-)^* \rightarrow Cl^- + Cl$	0	σ_4	k_4
Dissociative excitation	$e+Cl_2 \rightarrow (Cl_2)^* \rightarrow Cl + Cl + e$	3.12	σ_5	k_5
Atomic ionization	$e+Cl \rightarrow Cl^+ + e + e$	13.01	σ_6	k_6
	$e+Cl^+ \rightarrow Cl^{++} + e + e$	23.80	σ_7	k_7
Ion-ion recombination	$Cl_2^+ + Cl^- \rightarrow Cl_2 + Cl$			$k_8 \approx 5\times10^{-8}$
	$Cl^+ + Cl^- \rightarrow Cl + Cl$			$k_9 \approx 5\times10^{-8}$
Dissociative recombination	$Cl_2^+ + e \rightarrow Cl + Cl$			$k_{10} \approx 9\times10^{-7}/T_e^{0.6}$
Volume recombination	$Cl+Cl+M(Cl_2) \rightarrow Cl_2 + M(Cl_2)$			$k_v \approx 2.8\times10^{-32}$ cm^6/s
Wall recombination	$Cl+wall \rightarrow (1/2)Cl_2 + wall$			

for $E_e > 11.87$ eV, and $\sigma_4 = Q_a$ for $E_e < 11.87$ eV. Moreover, the cross section σ_5 for dissociative excitation of Cl_2 has been given by Rogoff *et al.* [13] through Boltzmann-equation calculations of electron swarm parameters for Cl_2; special attention will be given to this σ_5 later. From these cross sections σ_x (x=1–7), the corresponding rate coefficients k_x were evaluated as a function of T_e as shown in Fig. 5, assuming a Maxwellian electron energy distribution. It is noted here that the dissociative attachment, generating Cl^- negative ions and neutral Cl atoms, is significant ($k_4 > k_1$, k_5) at low T_e.

Cross sections or rate coefficients for the ion reactions are less well known. The ion-ion recombination rate for $Cl_2^+ + Cl^-$ has been measured to be $k_8 \approx 5\times10^{-8}$ cm^3/s at T=300 K [14]; the $Cl^+ + Cl^-$ recombination rate k_9 may also be large and comparable to k_8 for $Cl_2^+ + Cl^-$ [13]. The dissociative recombination rate for Cl_2^+ was taken to

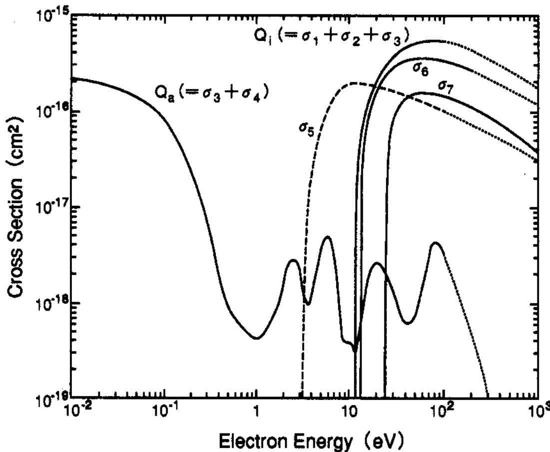

Fig. 4 Cross sections for electron-impact processes in chlorine that have been known in the literature: Q_i, the total ionization cross section for Cl_2; Q_a, the total cross section for negative ion formation from Cl_2; σ_5, the cross section for dissociative excitation of Cl_2; σ_6, the ionization cross section for Cl; and σ_7, the ionization cross section for Cl^+.

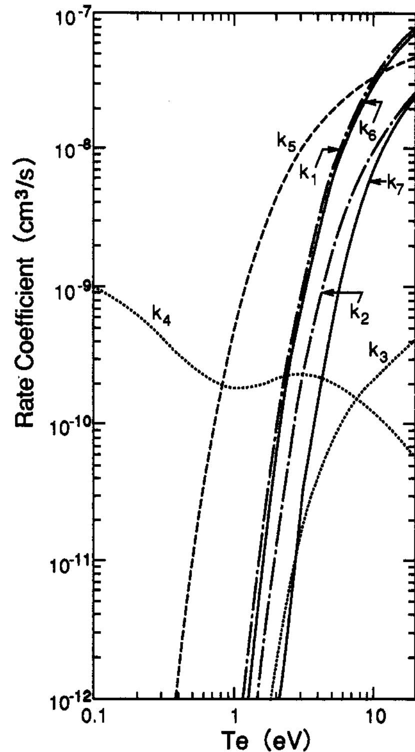

Fig. 5 Rate coefficients k_x (x=1–7) for electron-impact processes in chlorine as a function of electron temperature T_e, evaluated assuming a Maxwellian electron energy distribution.

be similar to that for Ar_2^+ at T=300 K [15]: k_{10}≈$9\times10^{-7}/T_e^{0.6}$ cm³/s with T_e in eV. In addition, as for ion reactions of chlorine, the cross section for Cl_2^++Cl_2 symmetric charge exchange has been given at high ion energies E_i>100 eV [16]; however, that for Cl^++Cl_2 asymmetric one, probably significant at low E_i, is not available. The cross section for Cl^-+Cl_2 asymmetric charge exchange has also been measured as a function of E_i, together with the electron detachment cross section for Cl^-+Cl_2 [17]. Such charge exchange processes were not taken into account in the present model, owing to their less effects on the chemical compositions.

As for loss mechanisms for neutral Cl atoms, the rate coefficient for gas-phase recombination has been measured to be k_v≈2.8×10^{-32} cm⁶/s at T=300 K [18]. Under low-pressure ECR plasma conditions, however, the neutral gas-phase chemistry is unimportant in view of small termolecular collision rates. As a result, diffusion to the chamber walls, where recombination and/or adsorption takes place, is the dominant loss process for Cl in ECR.

Given the measured n_e and T_e in Fig. 2(a) and the feedstock gas density $[Cl_2]_0$, a set of 5 steady-state rate equations for Cl, Cl_2^+, Cl^+, Cl^{++}, and Cl^- were solved numerically, together with 2 equations for charge neutrality and species conservation. The diffusion problem from the gas phase to the chamber walls was treated as a characteristic decay time: τ_n for neutral Cl was given by an approximation of Chantry [19] with the known diffusion coefficient D of Cl in Cl_2 [20]; $\tau_n = (\Lambda_0^2/D)+(V/A)2(2-\alpha)/v\alpha$, where Λ_0 is the diffusion length determined by the container geometry, V/A the volume-to-surface-area ratio of the container, v the thermal velocity of Cl, and α the sticking probability of Cl at the walls ($0\leq\alpha\leq1$). Assuming the specimen chamber to be a cylindrical container, the neutral decay time was evaluated to range from τ_n≈1.4 ms at P_0=10 mTorr to 0.083 ms at P_0=0.2 mTorr. It is noted that $\tau_n \ll \tau_r$, the gas residence time. The decay times τ_i for ions were taken to be the same for all ionic species. In the calculations thus achieved, the respective species concentrations $[Cl_2]$, [Cl], $[Cl_2^+]$, $[Cl^+]$, $[Cl^{++}]$, and $[Cl^-]$ were obtained with the ionic decay time τ_i.

The calculated and measured Cl concentrations are compared in Fig. 3(a). Here, the calculations were made assuming the sticking probability α=1 at the walls, that is, all Cl atoms onto the surfaces are recombined and/or adsorbed. Agreement between the calculated and measured values was not obtained when using the original rate coefficient k_5 or cross section σ_5 for dissociative excitation of Cl_2; in effect, the agreement was obtained by lowering σ_5 by about an order of magnitude. In the present comparison, the agreement is not sufficient at lower P_0<1 mTorr. However, it may be concluded that the presently known cross section σ_5 for dissociative excitation of Cl_2 is excessively large, by about an order of magnitude.

Figure 6 shows the chemical compositions in ECR Cl_2 plasmas, obtained numerically with $\sigma_5\times0.1$ as a function of pressure P_0. The ionic decay times calculated were between τ_i≈15 and 4.6 μs, decreasing with decreasing P_0. It may be noted that in our ECR plasmas, molecular Cl_2^+ ions are still more abundant than atomic Cl^+ ions; moreover, Cl^- negative ions are less abundant than plasma electrons, which is in contrast to the situation generally appreciated for rf discharges at high pressures [21].

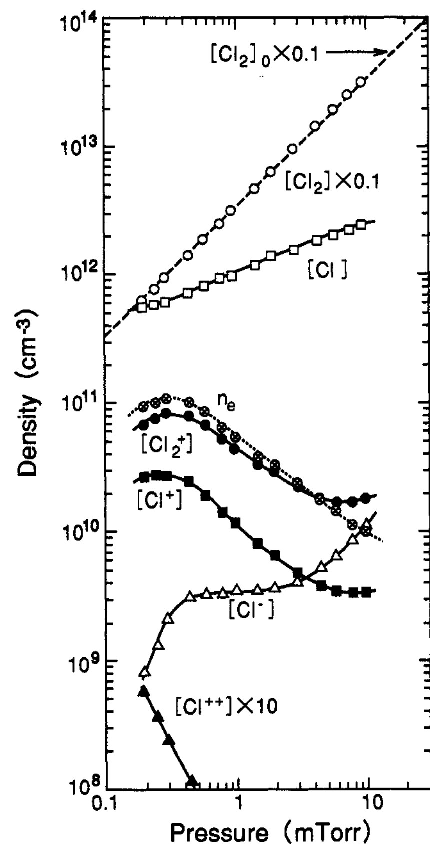

Fig. 6 Species concentrations $[Cl_2]$, [Cl], $[Cl_2^+]$, $[Cl^+]$, $[Cl^{++}]$, and $[Cl^-]$, obtained numerically with α=1 and $\sigma_5\times0.1$ for different Cl_2 pressures P_0. Also shown are the measured n_e and the feedstock gas density $[Cl_2]_0$.

5. Etch Rates and Profiles

Figure 7 shows the etch rate of polycrystalline Si as a function of Cl_2 pressure P_0, where the solid squares represent the measured data. In these experiments, poly-Si etch rates of 1000–2000 Å/min were obtained in combination with poly-Si/SiO_2 selectivities of >50. As P_0 is decreased, the etch rate increases, peaks at $P_0 \approx 0.5$ mTorr, and then decreases. This P_0 dependence is similar to that of the ion flux Γ_i onto the substrate in Fig. 2(c).

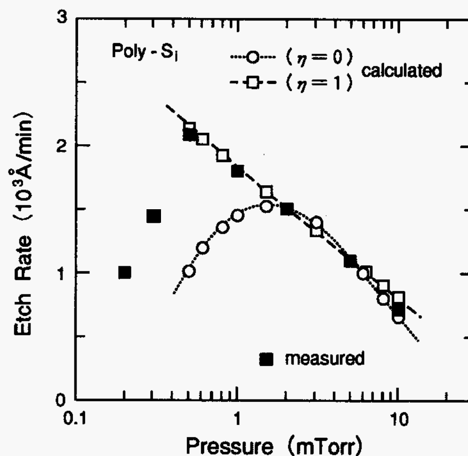

Fig. 7 Etch rate of polycrystalline Si as a function of Cl_2 pressure P_0. The solid squares are the measured data, while the open circles and squares represent the results from etch rate models taking account of an adsorption-reaction-ion stimulated desorption process.

In general, a simple ion-assisted reaction model [22] that accounts for the etch rate behavior assumes that the etch yield per ion is proportional to the ion energy E_i and the surface coverage Θ of reactive neutral species: $R = a\Theta E_i \Gamma_i$. Moreover, the reaction probability of neutrals is assumed to be proportional to the number of bare sites on the surface: $R = bS_0(1-\Theta)\Gamma_{Cl}$, where S_0 is the sticking probability on a bare surface. Thus, the etch rate R may be expressed as a function of ion energy and ion and neutral Cl fluxes as follows: $R = aE_i^{0.5}\Gamma_i / \{1+aE_i^{0.5}\Gamma_i/(bS_0\Gamma_{Cl})\}$, where the energy dependence is taken to be $E_i^{0.5}$ [1] because of low ion energies in ECR plasmas. Here, the two constants a and bS_0 may be determined from the measured data on R, E_i, Γ_i, and Γ_{Cl} under two different conditions, e.g., at P_0=3 and 5 mTorr. However, this expression could not fit the measured etch rates at lower pressures, $P_0 \leq 1$ mTorr, as shown in Fig. 7 with η=0. Under ECR plasma conditions where the ion-to-neutral flux ratio is large (Γ_i/Γ_{Cl}>1) and the ion energy is low (E_i<20 eV), we may assume that the incoming low-energy ions as well as neutrals are adsorbed on surfaces with the same S_0 to form reaction products; then, $R = aE_i^{0.5}\Gamma_i/[1+aE_i^{0.5}\Gamma_i/\{bS_0\Gamma_{Cl}(1+\eta\Gamma_i/\Gamma_{Cl})\}]$, where η=0 corresponds to adsorbate formation by neutrals only, and η=1 to by ions and neutrals. The expression thus assumed fits the measured etch rates over a relatively wide P_0 range, as shown in Fig. 7 with η=1; the disagreement at much lower P_0<0.5 mTorr could not be explained at the present stage.

The etched profiles obtained were nearly anisotropic with the photoresist largely intact over the P_0 range studied, as shown in Fig. 8, exhibiting no undercutting or signature of purely chemical etching; this is in contrast to the conventional and magnetron-enhanced reactive ion etching [23]. Such highly directional, highly selective etching in ECR is ascribed primarily to high ion-to-neutral flux ratios onto the substrate and to low energies of the incoming ions. In practice, however, some lateral etching like bowing and notching was observed after an overetch step particularly at higher P_0, as can be seen in (b) of this figure. The mechanism for such lateral etching in ECR may be the result of localized charging of pattern features [22,24,25]: differential charging occurs for insulating microstructures as a result of the differential angular distributions of incoming ions and electrons, and the electron charge establishes an electrostatic potential profile on the sidewalls that is large enough to affect the ion trajectories; thus, the incoming ions tend to be deflected laterally toward the sidewalls, striking near the bottom.

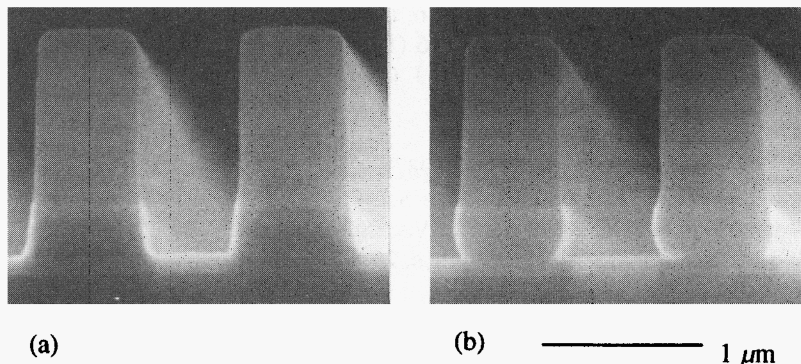

Fig. 8 SEM micrographs of the etched profile of polycrystalline Si after a 200 % overetch step, obtained at (a) P_0=0.5 mTorr and (b) P_0=1 mTorr.

6. Conclusions

Atomic chlorine concentrations in ECR Cl_2 plasmas have been measured by two-photon LIF technique. The Cl concentration ranged from [Cl] $\approx 2\times10^{12}$ to 3×10^{11} cm^{-3}, decreasing with decreasing pressure P_0; the corresponding Cl fractions, [Cl]/[Cl_2], were estimated to be between $\approx$ 1 and 2 %. These results, together with electrical measurements of ion and electron energies and densities, demonstrated that in ECR plasmas, the ratio of ion flux to neutral Cl flux toward the substrate is fairly high, $\Gamma_i/\Gamma_{Cl} > 0.1$, increasing almost linearly with decreasing P_0.

Chemical kinetics in Cl_2 plasmas have been modeled to gain an insight into the measured Cl concentrations and to understand chemical compositions in ECR plasmas. A comparison between the measured and calculated Cl concentrations indicated that the known cross section σ_5 for dissociative excitation of Cl_2 may be excessively large, by about an order of magnitude. The calculated chemical compositions showed that in ECR plasmas, molecular Cl_2^+ ions are still more abundant than atomic Cl^+ ions; moreover, Cl^- negative ions are less abundant than plasma electrons, which is in contrast to the situation generally appreciated for rf discharges at high pressures.

Under these ECR plasma conditions, poly-Si etch rates of 1000–2000 Å/min were obtained in combination with poly-Si/SiO_2 selectivities > 50. The etched profiles were nearly anisotropic, exhibiting no undercutting or signature of purely chemical etching; in practice, some lateral etching was observed after an overetch step, particularly at higher P_0. Such highly directional, highly selective etching in ECR is ascribed primarily to high ion-to-neutral flux ratios Γ_i/Γ_{Cl} onto the substrate and to low energies of the incoming ions. The etch rate behavior may be well expressed in terms of an adsorption-reaction-ion stimulated desorption process, assuming the incoming low-energy ions as well as neutrals to be adsorbed on surfaces. Moreover, the lateral etching in ECR may be interpreted in terms of the incoming ion trajectories affected by localized charging of pattern features.

The problems contained in this paper tend to be generic to all low-pressure, high-density plasma etching, although many of them remain unresolved.

References

1. W.M. Holber and J. Forster, J. Vac. Sci. Technol. A **8**, 3720 (1990).
2. J.L. Cecchi, J.E. Stevens, R.L. Jarecki, Jr., and Y.C. Huang, J. Vac. Sci. Technol. B **9**, 318 (1991).
3. N. Sadeghi, T. Nakano, D.J. Trevor, and R.A. Gottscho, J. Appl. Phys. **70**, 2552 (1991).
4. M.A. Hussein, G.A. Emmert, N. Hershkowitz, and R.C. Woods, J. Appl. Phys. **72**, 1720 (1992).
5. T. Oomori, M. Tuda, H. Ootera, and K. Ono, J. Vac. Sci. Technol. A **9**, 722 (1991); M. Tuda, T. Oomori, H. Ootera, and K. Ono, in *Proc. of the 3rd Japanese Symposium on Plasma Chemistry, Tokyo, 1990*, edited by A. Kanzawa (Organizing Committee of JSPC, Tokyo, 1990), pp. 165–170.
6. K. Ono, T. Oomori, M. Tuda, and K. Namba, J. Vac. Sci. Technol. A **10**, 1071 (1992); K. Ono, T. Oomori, and M. Tuda, Jpn. J. Appl. Phys. **31**, L269 (1992).
7. B. Chapman, *Glow Discharge Processes: Sputtering and Etching* (Wiley, New York, 1980), p. 69.
8. M.V. Kurepa and D.S. Belić, J. Phys. B **11**, 3719 (1978).
9. T.R. Hayes, R.C. Wetzel, and R.S. Freund, Phys. Rev. A **35**, 578 (1987).
10. I. Yamada, A. Danjo, T. Hirayama, A. Matsumoto *et al.*, J. Phys. Soc. Jpn. **58**, 3151 (1989).
11. J.A.R. Samson and G.C. Angel, J. Chem. Phys. **86**, 1814 (1987).
12. J. Berkowitz, C.A. Mayhew, and B. Ruščić, Chem. Phys. **123**, 317 (1988).
13. G.L. Rogoff, J.M. Kramer, and R.B. Piejak, IEEE Trans. Plasma Sci. **PS-14**, 103 (1986).
14. M.J. Church and D. Smith, J. Phys. D **11**, 2199 (1978).
15. M.A. Biondi, in *Applied Atomic Collision Physics: Vol. 3, Gas Lasers*, edited by E.W. McDaniel and W.L. Nighan (Academic, New York, 1982), Chap. 6, p. 178.
16. S.N. Ghosh and W.F. Sheridan, J. Chem. Phys. **27**, 1436 (1957).
17. M.S. Huq, D. Scott, N.R. White, R.L. Champion *et al.*, J. Chem. Phys. **80**, 3651 (1984).
18. R.K. Boyd and G. Burns, J. Phys. Chem. **83**, 88 (1979).
19. P.J. Chantry, J. Appl. Phys. **62**, 1141 (1987).
20. C.-J. Hwang and T.-M. Su, J. Phys. Chem. **91**, 2351 (1987).
21. M. Meyyappan and T.R. Govindan, IEEE Trans. Plasma Sci. **PS-19**, 122 (1991).
22. R.A. Gottscho, C.W. Jurgensen, and D.J. Vitkavage, J. Vac. Sci. Technol. B **10**, 2133 (1992).
23. K. Ono, T. Oomori, and M. Hanazaki, Jpn. J. Appl. Phys. **29**, 2229 (1990).
24. S.G. Ingram, J. Appl. Phys. **68**, 500 (1990).
25. J.C. Arnold and H.H. Sawin, J. Appl. Phys. **70**, 5314 (1991).